Emergent Scientist **3**, 2 (2019)

https://doi.org/10.1051/emsci/2019001

Emergent Scientist

Available online at:
www.emergent-scientist.edp-open.org

IPT 2018

RESEARCH ARTICLE OPEN ACCESS

From the microstructure of steels to the explosion of sparks

Anthony Guillen[1,*], Fang Goh[1], Julie Andre[1], Amaury Barral[1], Clement Brochet[1], Quentin Louis[1], and Thibault Guillet[2]

[1]Ecole polytechnique, Route de Saclay, 91120 Palaiseau, France

[2]LadHyX, UMR 7646 du CNRS, Ecole polytechnique, 91128 Palaiseau Cedex, France

Received: 13 July 2018 / Accepted: 2 January 2019

Abstract. Sparks ejected by the grinding of steel can be observed to split in mid-flight. In this paper, we investigate the link between steel microstructure and the splitting behavior using two different steels: hypoeutectoid (containing less than 0:8% carbon) and hypereutectoid (>0:8% carbon). We used a high-speed camera filming at 1000 fps to observe the sparks, and a Scanning Electron Microscope to image the microstructures. For the hypoeutectoid steel, we also quantified the splitting behavior of the sparks by measuring the statistical distribution of the linear distance they travel before splitting occurs. We find that our results are coherent with the common explanation of the splitting phenomenon, stating that sparks split because their microstructures allow the formation of pockets of CO_2 by oxidation of Fe_3C, producing an internal pressure and leading to explosion.

Keywords: Metallurgy / steel / microstructure / sparks / explosion

1 Introduction

When an angle grinder is applied to metal, small metal particles are ejected. These particles can oxidize, from the heat generated by oxidation, become hot enough to glow; we then call them sparks. The hot sparks then cool down due to convective and radiative cooling. They quickly become invisible to the naked eye when the rate of cooling exceeds the rate of oxidation, which decreases over time because of the formation of a protective oxide layer on the surface which impedes oxygen diffusion [1,2]. Not all alloys create sparks when grinded. For instance, copper and aluminum do not, but steel and titanium do; Kelley [3] has done a complete study of the radiance of metal grinding sparks and gives some reasons to explain these observations.

As steel sparks fly in the air, it is observed that they explode or split, which appear to the naked eye as little forks at the end of their glowing trail. These splittings can occur because of the inhomogeneous distribution of carbon inside the sparks [4]. Indeed, their microstructures allow the formation of pockets of carbon dioxide inside the spark, produced by the oxidation of cementite (Fe_3C). The pressure of these pockets of gas then rises until the internal force is large enough to break the brittle oxide layers, producing an explosion [5]. Hence, there is a link between the microstructural composition of steels, most importantly their microstructures, and the splitting behavior of the sparks they produce. The characteristics of the sparks, namely, the distance they travel before they stop glowing, their splitting behavior and their color can be used to identify metals [6]. However, these previous investigations are mainly empirical methods; accordingly the purpose of this paper is to further investigate the relationship between the microstructures of the steels and the behavior of the sparks.

2 Methods

To observe the sparks, we used the setup shown in Figure 1. On the right hand side of the picture, the angle grinder (wheel diameter 10 cm, power 850 W) is fixed to a table. A steel bar is attached to the apparatus shown on the diagram on the right of the picture. On this apparatus, the steel bar is basically a lever and the condition of equilibrium $Mgl_1 = F_2 l_2$ enables us to control the force F_2 applied on the grinder by changing the mass M and the distance from the pivot l_1. We used as forces 50, 75 and 100 N.

On the left hand side of the picture, about 1 m from the grinder, a high speed camera is shown, this is used to record the motion of the sparks at 1000 fps. The camera is positioned perpendicularly to the plane of the trajectory of the sparks. We placed a dark background behind the sparks to enhance their visibility.

Finally, we used two commercial steels with different carbon concentration: a hypoeutectoid one (0.17 ± 0.01%C) and a hypereutectoid one (1.15 ± 0.05%C).

* e-mail: anthony.guillen@polytechnique.edu

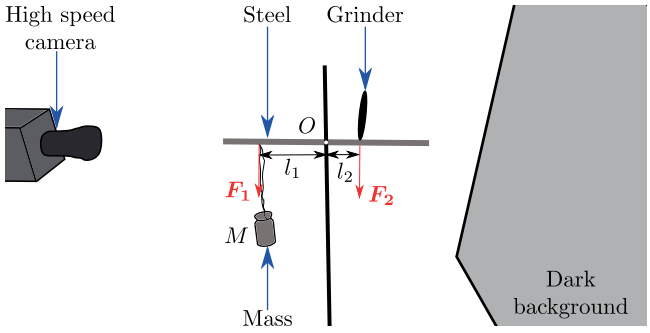

Fig. 1. Setup for sparks observation.

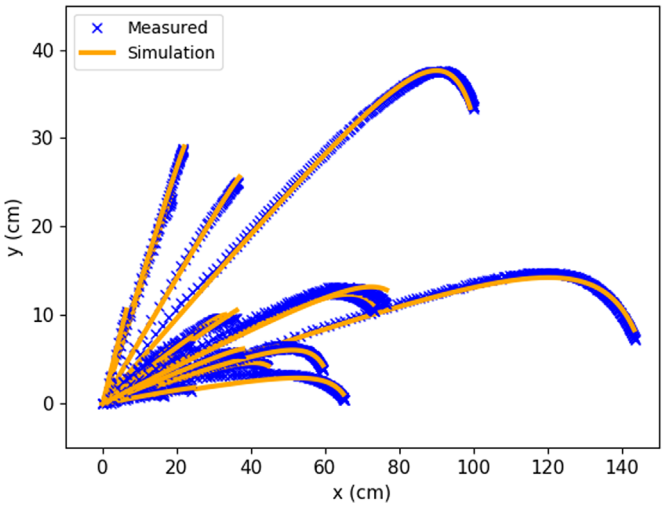

Fig. 2. Measured trajectories of sparks and fittings of the equation of motion, for 30 sparks of the hypoeutectoid steel with 100 N applied to the grinder; x and y are the spatial directions of the image.

2.1 Method to measure sparks' radius and initial velocity

Since sparks are too small to be resolved by our high speed camera, we designed a mechanical method to extract the radius and velocity distribution from the trajectory of the sparks. If we assume that sparks are only affected by their weight and air resistance when they fly in air, we can write the equation of motion for their velocity V as:

$$m\frac{d\mathbf{V}}{dt} = m\mathbf{g} - \frac{1}{2}\rho_{\text{air}} S C_x(V,R) V^2 \mathbf{e_V}, \tag{1}$$

where $\mathbf{g}$ is the gravity force and $\mathbf{e_V}$ the unit vector along the trajectory, m the mass, ρ_{air} the density of air, S the cross section of the spark of radius R and $C_x(V,R)$ the drag number, a function of the speed and geometry of the sparks. Assuming that the sparks are spherical and that S depends only on R, and m depends only on R and the density of steel; C_x can be expressed as a function of the Reynolds number Re, a ratio of inertial forces to viscous forces in a fluid flow:

$$\text{Re} = \frac{\rho_{\text{air}} R V}{\eta_{\text{air}}}. \tag{2}$$

Here, ρ_{air} and η_{air} are respectively the density and the dynamic viscosity of air. For the sparks, the regime of the flow is intermediate between laminar and turbulent ($\text{Re} \approx 30$); so, we will use Allen's law [7] for the drag coefficient:

$$C_x = \frac{18.5}{\text{Re}^{0.6}}. \tag{3}$$

Combining equations (1), (2) and (3), we can see that the only unknown parameters in the equation of motion are the radius R and the initial velocity $\mathbf{V_0}$ of the sparks. Hence, by tracking the trajectories of individual sparks and using Python to fit the equation of motion on these two parameters, as shown in Figure 2, we were able to estimate values of R and V_0; we obtained those values for 30 individual sparks of the hypoeutectoid steel for each of three different forces applied to the grinder (50, 100 and 150 N). It was important to know the typical size of sparks in order to compare with the sizes of the microstructures.

Note that we neglected the motion in the direction perpendicular to grinding, since the path of sparks is mainly planar.

We did not do this study for the hypereutectoid steel though, because it quickly appeared to us that sparks' behaviors are much more complicated in this case (see Fig. 3). In fact, hypereutectoid usually splits multiple times and constantly emits tiny sparks around them, making it wrong to apply equation (1) on them.

2.2 Method to detect sparks and explosions

In our study, we were interested in characterizing the splitting behavior of the sparks. One of the most straightforward things to do so was measuring the distance distribution of the explosions, and to compare it with the distance distribution of sparks, for different forces applied.

By distance distribution of the sparks, we mean the statistical distribution of the distance they travel before they do not glow enough anymore to be detectable with our camera; and by distance distribution of the explosions, we mean the distribution of the distance they travel before exploding. The distances considered in both case are linear distances measured from the contact point of the angle grinder and the steel bar. It should be noted that the distribution obtained only accounts for distances larger than 40 cm since individual sparks are nearly indistinguishable for shorter distances as seen from Figure 4.

To measure the distance distribution of the sparks, we used an image analysis software, ImageJ [8], to detect the pixels with maximum intensity on an image. We then use a script to process each frame of the videos.

The process of obtaining the distance distribution of explosions is more delicate. Since sparks exhibit a large variety of behaviors, especially for the hypereutectoid steel, we decided to limit the distribution study to

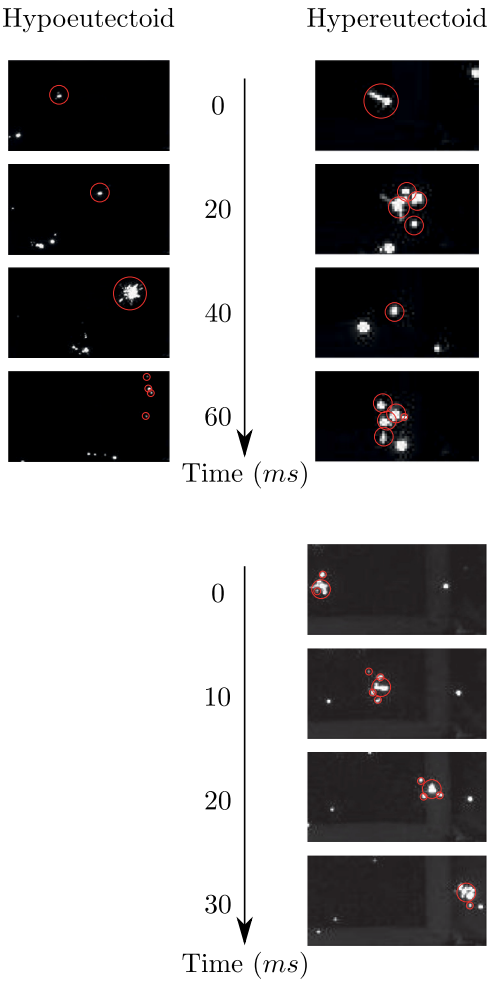

Fig. 3. Different morphologies of splitting: left, explosion of an hypoeutectoid spark; top right, double explosion of an hypereutectoid spark; bottom right, constant emission of tiny sparks around an hypereutectoid spark. The sparks circled in red are the products of a single spark.

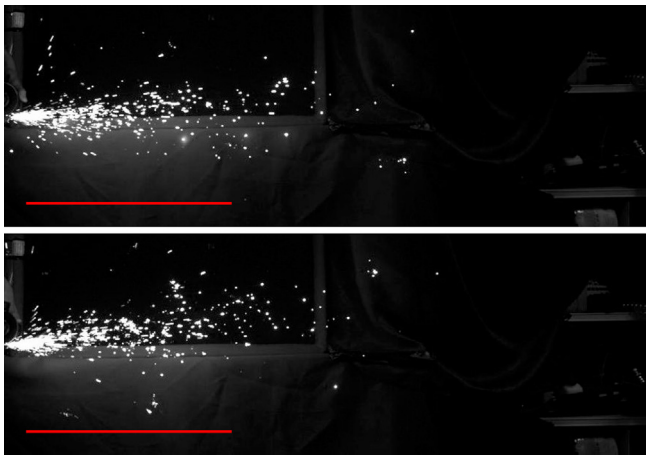

Fig. 4. Images taken by the high speed camera, showing the typical flow of sparks; hypoeutectoid (top) and hypereutectoid (bottom) steel, 100 N. The red line represents 50 cm.

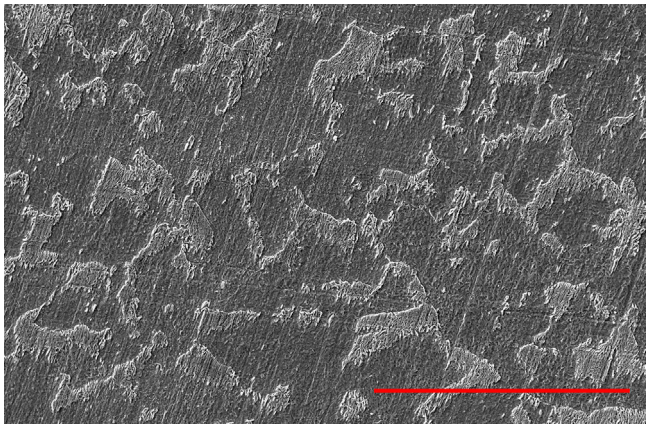

Fig. 5. SEM image of the hypoeutectoid steel: dark gray, ferrite; light gray, pearlite. The red line represents 40 μm.

hypoeutectoidal steel, which allowed us to define explosions with three main characteristics: (1) the bursting of a spark with high light intensity followed by (2) a significant deviation from the spark's initial trajectory and (3) its rapid dimming afterwards. These three characteristics allow us to exclude the little bursts on the surface of the sparks which we think occurred due to other phenomena.

2.3 Method to observe the microstructures

To observe the microstructure of the steels, we used a Scanning Electron Microscope (SEM), allowing us to reach a magnification factor over 2500. Following the usual protocol, we first polished a small section of the steels to obtain a smooth surface with an average grain size of around 1 μm. We then submerged the metal pieces into nitric acid which revealed the microstructures by reacting differentially with the various phases of the steel when applied for an appropriate period of time; a process similar to chemical etching. An example is given in Figure 5.

3 Results

3.1 Measurement of sparks' radius and initial velocity

A histogram of the measured radii and initial speeds is shown in Figure 6, for an applied force of 500 N. The measured average values and standard deviation for radius and initial velocity are given in Table 1 for hypoeutectoid steel and different forces. For both parameters, we observe no clear dependence of the average values on the force applied to the grinder; however, we observed that more sparks were produced with an increased force. We also observed little correlation between R and V_0. These values were measured with 30 sparks for each force. Also, the average initial velocity measured for the sparks is close to the tangential speed of the grinding disk, which is $V_0 = 34\,\mathrm{ms}^{-1}$.

Thereafter, we may use this value of $R = 50\,\mu$m as a typical radius for the sparks in order to compare with the size of the microstructures of steel.

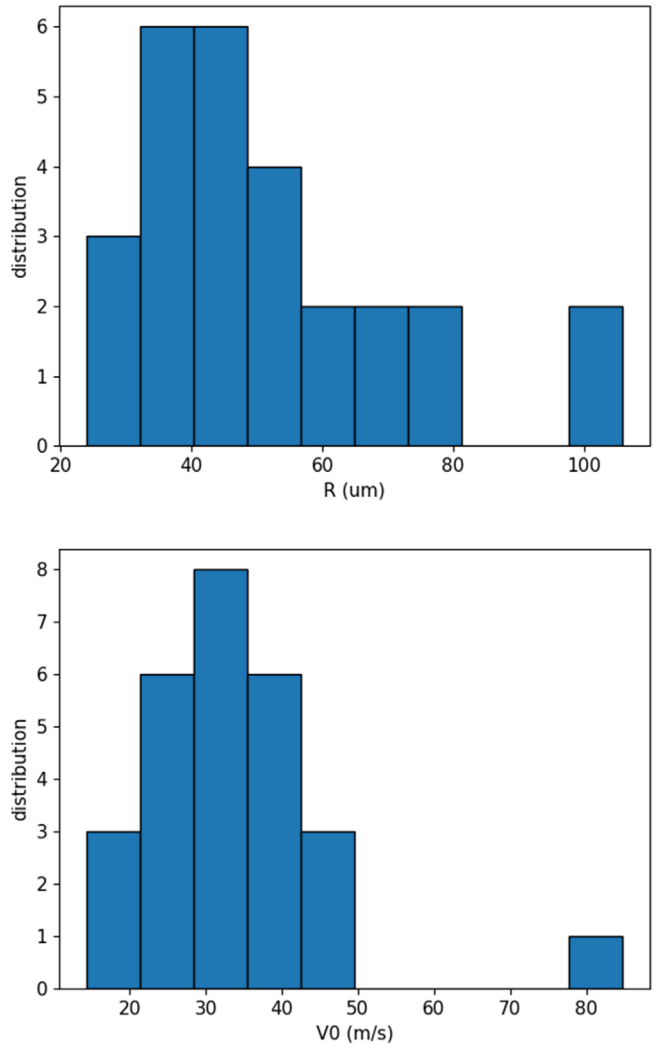

Fig. 6. Histogram of the radii (top) and initial speeds (bottom), for 30 sparks of the hypoeutectoid steel with 100 N applied.

Table 1. Average values and standard deviation of sparks' radius and initial velocity (hypoeutectoid steel). Tangential speed of the grinder disk is 34 ms^{-1}.

Force (N)	R (μm)	V_0 (ms^{-1})
50	50 ± 20	30 ± 10
75	50 ± 10	40 ± 9
100	50 ± 20	33 ± 5

3.2 Observations of splittings

From the videos taken by the high speed camera, we observed splittings for both steels. An illustration of this phenomenon is shown on Figure 3. However, the morphology of the splittings is much different for the two steels. Most of the hypoeutectoid sparks split only once and rapidly, which resembles an explosion. Sometimes, they emit a burst of light before doing so.

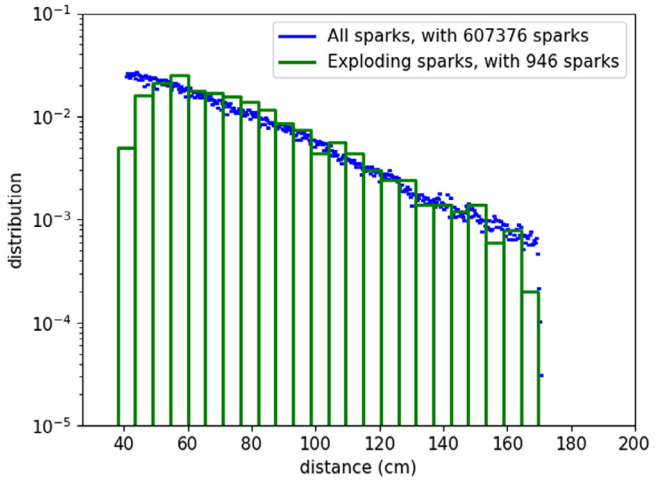

Fig. 7. Distance distribution of the sparks (blue) and explosions (green) for the hypoeutectoid steel with 100 N applied. We represented only the top of the bars for the distribution of the sparks for readability reasons.

On the other hand, hypereutectoid sparks split multiple times along their path, and exhibit various behaviors. The majority of them constantly emit small sparks all around them. Some of them also produce explosions. Very rarely, we could observe multiple explosions for an individual sparks, and even explosions of fragments produced from a previously exploded spark. Because of the complexity of these behaviors, we were unable to unequivocally define the splittings for this steel, let alone measure the distance distribution of these splittings as we had done for the hypoeutectoid steel.

3.3 Distance distribution of the sparks and explosions

The distance distribution of the sparks and of the explosions for the hypoeutectoid steel is shown in Figure 7, the plot of these two distributions for an applied force of 100 N. As defined before, by distance distribution of the sparks, we mean the statistical distribution of the distance they travel before they do not glow enough anymore to be detectable with our camera; and by distance distribution of the explosions, we mean the distribution of the distance they travel before exploding; both distributions start from 40 cm because below this distance, the concentration of sparks is too high to allow us to distinguish the individual sparks from the rest. In order to represent the two distribution on the same graphic, since there are much more data points for the distance distribution of sparks than for the distribution of explosions, we normalized them both so the area below the curves equals 1; this will have little impact on the following study.

The vertical scale being logarithmic, the linear graph obtained means that the distribution is exponential:

$$f(d) \propto \exp\left(\frac{-d}{\lambda}\right) \tag{4}$$

Table 2. Characteristic length λ in cm of the distribution for different forces applied.

	λ (cm)	
Force applied (N)	Sparks	Explosions
50	23.8 ± 0.4	24 ± 2
75	25.5 ± 0.3	24 ± 2
100	30.9 ± 0.3	33 ± 2

More importantly, we observe that the distributions of the sparks and of the explosions coincide quite well; and this remains true for the various forces applied. We can further confirm this observation by looking at the characteristic length λ of the exponential graphs shown in Table 2. From the table, we can also see that this length, which can be considered as the spatial extension of the sparks flow, increases with the force applied; this will be discussed in the following section.

3.4 Microstructures

An image from SEM of the hypoeutectoid steel is given in Figure 5. We can clearly see that the steel is inhomogeneous at the microscopic level with two distinct phases. The dark grey phase is Ferrite, another name for α iron. The light gray regions are grains of pearlite, which is a two-phase lamellar compound of ferrite and cementite; however, our SEM has insufficient magnification to distinguish the two from one another [4]. Cementite is a solid precipitate of carbon in iron, of formula Fe_3C. The scale of these microstructures is given by the red line, which represents 40 μm. Comparing this with the typical radius of the sparks which measures as 50 μm, we conclude that carbon is unevenly distributed in the sparks.

4 Discussion

4.1 Independence of sparks' radius and initial velocity with the applied force

For the radius and initial velocity of the sparks, we observed no clear dependence on the force applied. Therefore, we think that the radius of the sparks depends on others parameters, such as the metal used and the roughness of the grinder. For instance, we think that if the metal is more brittle, it will produce bigger particles; and if the grinder is smoother, it will produce smaller particles.

Also, we observed that the average initial speed of the sparks ejected is close to the tangential speed of the grinder at contact point; so this tangential speed may be the most important parameter controlling the initial speed of the sparks. But we observe on histogram of Figure 6 that some sparks can be ejected much more rapidly than this tangential speed. We think this is due to the possibility of elastic energy to be stored locally in steel during grinding. But the complexity of the deformations involved in the grinding processes did not allow us to go further in this investigation.

Fig. 8. Comparison of the sparks produced by grinding in a chamber filled with air (left) and with neon (right)

4.2 Increase of λ with the applied force

The spatial extension of the flow of sparks increases with the force applied. However, we also measured that the initial velocity of the sparks does not depend on this parameter, so the ejected metal particles may not actually go further. To explain this, we suggest that, if we increase the force applied, sparks are produced at a higher temperature, allowing them to remain observable for a longer distance.

Nevertheless, oxidation remains the main source of heat for the sparks; we showed it experimentally by grinding steel in a box filled with neon instead of air. As we see in Figure 8, in the absence of oxygen, we barely observe dim sparks. In the same figure, one can also observe that in the presence of oxygen, sparks glow more a after having travelled a few centimeters; meaning that they are, at first, getting hotter with time. Both these observations highlight the importance of oxidation; so the likely increase in initial temperature with the force applied counts only as an additional contribution to the temperature evolution of the sparks.

4.3 The splitting phenomenon

A common explanation [5], for the splitting phenomenon is that, with diffusion of oxygen into the sparks, the cementite contained in pearlite can oxidize according to the equation $Fe_3C + 3O_2 = Fe_3O_4 + CO_2$, which produces carbon dioxide. The carbon dioxide then accumulates inside the spark until its pressure is high enough to break the spark. This process is illustrated in Figure 9.

This explanation is consistent with our observations. Firstly, we have seen from the microstructures that carbon is localized in the sparks; so, the pockets of carbon dioxide can indeed form inside. In addition, we observed that the explosions of the sparks occur randomly; in the sense that, at any given time, the next spark to explode seems to be picjked uniformly among all the remaining sparks, as a Markovian process. This randomness we observed in the explosions can be explained by the distribution of the microstructures. The typical radius of sparks is comparable to the typical lengths of the microstructures; so, the composition of each spark can vary dramatically from one to the other. Some sparks can contain exclusively pearlite and others exclusively ferrite.

Furthermore, the differences observed in sparks' behavior for hypoeutectoid and hypereutectoid steel are directly correlated to the different microstructures of these

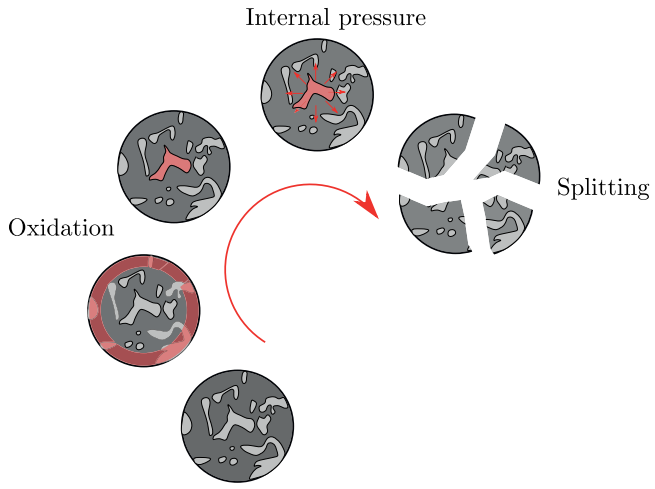

Fig. 9. Explanation of the splitting phenomenon. Dark gray, ferrite; light gray, pearlite; red, oxidation.

two steels. In fact, in hypereutectoid steel, the grains of pearlite are enclosed in a matrix of cementite instead of ferrite. From that, we should expect more splitting, and this is exactly what we observed, for instance in Figure 4. The abundance of cementite also explains why multiple splitting could occur for a single spark, as well as the more erratic behavior.

5 Dead end

5.1 Temperature of the sparks

Throughout our study, we tried to measure the temperature of the sparks, as it would have given us insights into the state of the sparks. We tried to use a thermal camera; however, despite filming very close to the contact point, the temperature measured was significantly lower than the expected values. Indeed, the camera was showing an average temperature of a given area of vision for some acquisition time. We also tried to obtain the temperature indirectly by measuring the lifetime of sparks and doing a reverse calculation, taking into account the simultaneous oxidation and cooling process, but it was unfruitful. Finally, we tried to use a spectrometer to measure sparks' temperature considering them as blackbodies, but we were not able to get any measurement because of the too strong directivity of our device. We did not investigate further, but it would be an interesting thing of study in order to have a fuller understanding of the physics of sparks and to be able to simulate their flow.

6 Conclusion

The aim of this work was to draw a link between the microstructures of steels and the splitting behavior of the sparks created from it. We investigated this link in detail for a sample of hypoeutectoid steel and showed that the common explanation for the explosion of sparks is consistent with our observations. Moreover, we observed that sparks' behaviors vary a lot between hypoeutectoid and hypereutectoid steels, which have indeed a very different microstructure. Further experiments will be undertaken using other steel samples in order to confirm the proposed link. This approach could lead to better identification methods in metallurgy.

The authors thank the laboratory LadHyx of Ecole Polytechnique for providing the materials and equipements to conduct the experiments. The authors also grateful to their team leaders: Thibault Guillet, Guilhem Gallot and Fabian Cadiz, respectively, from LadHyX, LOB and PMC, Ecole Polytechnique and their team mates from IPT 2018 for their constructive comments and suggestions throughout this study.

References

1. K.R. Lawless, The oxidation of metals, Rep. Prog. Phys. **37**, 231–316 (1974)
2. A. Bruckman, The mechanism of transportation of matter through the scales during oxidation of metals and alloys, Corros. Sci. **7**, 51–54 (1967)
3. J.E. Kelley, Studies of the radiance of metals and alloys, Thesis, Oregon state University, 1974
4. M.F. Ashby, D.R.H. Jones, Matériaux: microstructures et procédés de mise on oeuvre, Dunod, 2014
5. R.W. Buzzard, The utility of the spark test as applied to commercial steels, Bur. Stand. J. Res. **11**, 527–540 (1933)
6. Tschorn, Gerhart, Spark atlas of steels: cast-iron, pig-iron, ferro-alloys and metals, 1963
7. H.S. Allen, The motion of a sphere in a viscous fluid, **50**, 323–338 (1900)
8. J. Schindelin, I. Arganda-Carreras, E. Frise et al., Fiji, an open-source platform for biological-image analysis, Nat. Methods **9**, 676–682 (2012)

Cite this article as: Anthony Guillen, Fang Goh, Julie Andre, Amaury Barral, Clement Brochet, Quentin Louis, Thibault Guillet, From the microstructure of steels to the explosion of sparks, Emergent Scientist **3**, 2 (2019)